The Astrophysical Journal, 983:140 (11pp), 2025 April 20 https://doi.org/10.3847/1538-4357/adc376

CY Aquarii: A Triple System with Twin Companions

Ming Lian (连茗)[1,2], Jia-Shu Niu (牛家树)[1,2,3], and Hui-Fang Xue (薛会芳)[4,5,6]
[1] Institute of Theoretical Physics, Shanxi University, Taiyuan 030006, People's Republic of China; jsniu@sxu.edu.cn
[2] State Key Laboratory of Quantum Optics Technologies and Devices, Shanxi University, Taiyuan 030006, People's Republic of China
[3] Collaborative Innovation Center of Extreme Optics, Shanxi University, Taiyuan 030006, People's Republic of China
[4] Department of Physics, Taiyuan Normal University, Jinzhong 030619, People's Republic of China
[5] Institute of Computational and Applied Physics, Taiyuan Normal University, Jinzhong 030619, People's Republic of China
[6] Shanxi Key Laboratory for Intelligent Optimization Computing and Blockchain Technology, Jinzhong 030619, People's Republic of China
Received 2024 December 14; revised 2025 March 5; accepted 2025 March 17; published 2025 April 16

Abstract

In this study, we conducted a comprehensive analysis of the SX Phoenicis (SX Phe) type star CY Aquarii (CY Aqr). Our investigation included a detailed $O-C$ analysis based on a 90 yr observational data set, augmented by 1367 newly determined times of maximum light. The $O-C$ diagram reveals that (i) the primary star of CY Aqr exhibits a linear period variation rate of $(1/P_0)(dP/dt) = (2.132 \pm 0.002) \times 10^{-8}\,\mathrm{yr}^{-1}$ for its dominant pulsation mode; (ii) the primary star is disturbed by two companions and part of a triple system; (iii) Companion A has an orbital period of approximately 60.2 yr and Companion B has an orbital period of approximately 50.8 yr. It is highly probable that both Companion A and B are white dwarfs, with Companion A's elliptical orbit displaying an eccentricity of $e = 0.139 \pm 0.002$, which is the lowest confirmed value in similar binary and triple systems to date. Most notably, Companion A and B have masses that are identical within the uncertainties, with a mass ratio exceeding 0.99. Whether this is considered a coincidental event or the result of an underlying mechanism, CY Aqr is an exceptionally rare case that broadens our understanding of multiple star systems and offers a unique opportunity to delve into the enigmatic evolutionary histories of such configurations. Further intriguing characteristics of this system warrant investigation in future studies, based on additional observational data.

Unified Astronomy Thesaurus concepts: SX Phoenicis variable stars (1673); Pulsating variable stars (1307); Trinary stars (1714)

Materials only available in the online version of record: machine-readable table

1. Introduction

SX Phoenicis (SX Phe) variables, characterized as short-period pulsation stars residing within the classical Cepheid instability strip, are distinguished by their low metallicity and high spatial velocity (D. H. McNamara 1995). These high-amplitude δ Scuti stars (HADS) of Population II display variability, marked by either single or double radial modes and significant pulsation amplitudes (X. H. Yang et al. 2012; J. Daszyńska-Daszkiewicz et al. 2020; J.-S. Niu et al. 2023), akin to those observed in HADS (J.-S. Niu et al. 2017; H.-F. Xue et al. 2018, 2022; D. M. Bowman et al. 2021; J.-S. Niu & H.-F. Xue 2022; J. Daszyńska-Daszkiewicz et al. 2023, 2024; W. Xue et al. 2023). The SX Phe variables, with masses ranging from 1.0 to 1.2 $M_\odot$ and ages spanning approximately 2–5 Gyr (J. Nemec & M. Mateo 1990), present an enigmatic origin and evolutionary mechanism, with hypotheses suggesting a possible genesis through the merger of close binary stars (M. Breger 2000). Consequently, the examination of SX Phe stars within binary and multiple star systems is crucial for unraveling their formation and evolutionary narratives.

CY Aquarii (CY Aqr; $\langle V \rangle = 11.04$ mag, spectral type: A2-A8, [Fe/H] = −1.5; D. H. McNamara et al. 1996) represents an SX Phe variable star in the post-main-sequence phase of evolution (G. K. Andreasen 1983), initially discovered by Hoffmeister (A. Jensch 1934) and subject to extensive, long-term observations (for example, see O. Struve 1949; R. H. Hardie & C. R. Tolbert 1961; R. E. Nather & B. Warner 1972). While confirmed as a radial single-mode pulsating star (W. Xue et al. 2023), the specific mode of pulsation, whether fundamental or overtone, remains uncertain (D. H. McNamara 1995; J. H. Peña et al. 1999).

Regarding the period variation of CY Aqr, R. H. Hardie & C. R. Tolbert (1961) noted a subsequent decrease in the star's period during the 1950s. J. R. Percy (1975) later concluded that the period was stable between 1934 and 1951, with a significant alteration in 1951. As research into the period variation persisted, multiple theories emerged to account for this phenomenon (H. A. Mahdy & B. Szeidl 1980; B. C. Kamper 1985; J. M. Powell et al. 1995). With the aggregation of photometric data, the prevailing explanation for CY Aqr's period variation shifted to the light-travel time effect (LTTE) within a binary star system (D. W. Coates et al. 1994; J. N. Fu & C. Sterken 2003; A. Derekas et al. 2009). Nevertheless, periodic structures in the $O-C$ diagram residuals demand attention (J. N. Fu & C. Sterken 2003). W.-J. Fang et al. (2016) posited that the target star resides within a triple system, with the orbital periods of the two companion stars A and B determined to be 54.2 and 47.3 yr, respectively.

On one front, photometric observations of CY Aqr have been ongoing, particularly the high-precision, continuous data from the Transiting Exoplanet Survey Satellite (TESS),[7] which will not only elucidate further pulsation properties of the primary star but also yield more precise times of maximum light (TML). Concurrently, contemporary numerical frameworks enable a more rational and precise determination of the

[7] https://tess.mit.edu/science/

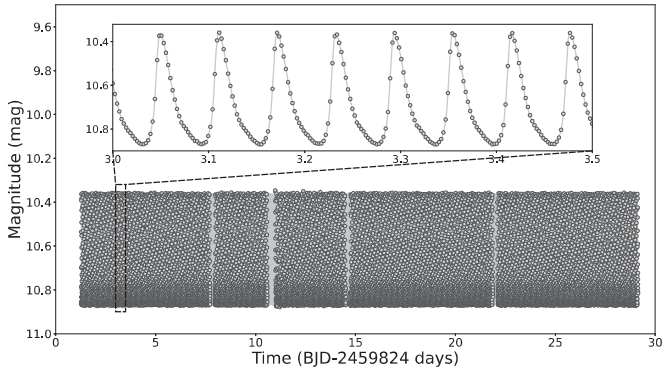

Figure 1. Light curve of CY Aqr (TESS Sector 56). The data points are represented by dots, and the gray line indicates the curve fitted using 22 extracted frequencies. The top panel displays a zoomed-in area covering 0.5 days.

system's orbital parameters (H.-F. Xue & J.-S. Niu 2020). Thus, it is apt to revisit this system.

2. Methods and Results

2.1. Pulsation Analysis

The TESS is a NASA mission dedicated to the detection of transiting exoplanets through an all-sky survey. CY Aqr was observed by TESS at a 120 s cadence during Sector 42 (2021 August) and at a 200 s cadence during Sectors 56 (2022 September) and 70 (2023 September). The data from these observations are accessible from the Mikulski Archive for Space Telescopes (MAST).[8] The Presearch Data Conditioning Simple Aperture Photometry (PDCSAP) flux was converted to magnitudes utilizing the TESS magnitude system (J. C. Smith et al. 2012; M. C. Stumpe et al. 2012, 2014; K. G. Stassun et al. 2019). The light curves of CY Aqr from TESS Sector 56 are depicted in Figure 1.

The prewhitening process of the light curves (TESS Sector 56) was executed using the Period04 software (P. Lenz & M. Breger 2005). The light curves were modeled with the following formula:

$$m = m_0 + \sum a_i \sin[2\pi(f_i t + \phi_i)], \tag{1}$$

where m_0 is the zero-point magnitude, a_i is the amplitude, f_i is the frequency, and ϕ_i is the corresponding phase. We applied a signal-to-noise ratio (S/N) threshold of greater than 5.6 as the criterion for frequency significance (J.-S. Niu & H.-F. Xue 2022; J.-S. Niu et al. 2023).

After the removal of alias frequencies, 22 statistically significant frequencies were identified, comprising 5 independent frequencies and 17 harmonics/combinations. For further details, refer to Figure 2 and Table 1.

2.2. Pulsation Mode Identification

The pulsation constant Q is defined by the formula:

$$Q = P\sqrt{\frac{\bar{\rho}}{\bar{\rho}_\odot}}, \tag{2}$$

where P represents the pulsation period, $\bar{\rho}$ is the mean density of the star, and $\bar{\rho}_\odot$ is the mean density of the Sun. Given the difficulty in directly detecting the mean density of stars, their pulsation constants Q are derived using the following relationship (M. Breger 1990):

$$\log Q = \log P + 0.5\log g + 0.1M_{\rm bol} + \log T_{\rm eff} - 6.456. \tag{3}$$

As the pulsation constant Q is sensitive to surface gravity and effective temperature (A. Poro et al. 2024), we employed two models—the TESS Input Catalog and Gaia DR3—as illustrated in Table 2—to ascertain Q (K. G. Stassun et al. 2019; Gaia Collaboration et al. 2021).

The absolute magnitude M_V is calculated using the equation:

$$M_V = V - 5\log d + 5 - A_V, \tag{4}$$

and the absolute thermal magnitude $M_{\rm bol}$ is determined according to J. O. Petersen & J. Christensen-Dalsgaard (1999):

$$M_{\rm bol} = M_V + {\rm BC}, \tag{5}$$

where the bolometric correction ${\rm BC} = 0.128\log P + 0.022$.

Ultimately, two new values of Q based on f_0 were derived: 0.0370 ± 0.0049 days and 0.0271 ± 0.0011 days, whose uncertainties are estimated based on the parameters from the TESS Input Catalog and Gaia DR3. Both values fall within the range indicative of the fundamental mode for such stars ($\geqslant$0.027 days; A. Poro et al. 2024).

However, the Q values derived here cannot exclude the possibility that the dominant mode could be the first overtone mode, even more so that the period ratio of F14 (f_2) to F1 (f_0) is indicative of the period ratio of the second to first radial overtone in HADS. It needs to be addressed in detail with the help of the asteroseismology models in a later part of this work.

In Table 2, we have also compiled results from historical literature.

2.3. O − C Analysis

Given that the amplitude of f_0 exceeds that of the other four independent frequencies by approximately 2 orders of magnitude and the light curves of CY Aqr are dominated by f_0, we employed the classical $O-C$ analysis to glean detailed insights into the primary star's period variations through the TML of the light curves.

We sourced the TML from four distinct origins: W.-J. Fang et al. (2016), C. Wiedemair et al. (2018, 2020), TESS, and the American Association of Variable Star Observers (AAVSO). Following the elimination of outlier data points, all data sets were converted to Barycentric Julian Dates (BJD) utilizing the Astropy Time package[9] and an online conversion tool.[10]

In total, we collected 2228 TML records, covering a period of approximately 90 yr from 1934 to 2023 (refer to Table B1 in Appendix B), which includes 1367 TML newly acquired in addition to those reported by W.-J. Fang et al. (2016). This extensive data set offers an unparalleled opportunity to investigate the period variation of the primary star and potentially the properties of its companions.

Specifically, 864 TML were directly extracted from W.-J. Fang et al. (2016), with three TML instances (HJD: 2439374.6443, 2438660.0051, and 2443815.3636) excluded due to significant deviations. An additional 41 TML were sourced from C. Wiedemair et al. (2018, 2020). Each of the 1142 TML from the three TESS Sectors was obtained by a fourth-order

[8] M. Lian (2025), doi:10.17909/3gqn-pz22.

[9] https://docs.astropy.org/en/stable/time/index.html

[10] https://astroutils.astronomy.osu.edu/time/, J. Eastman et al. (2010).

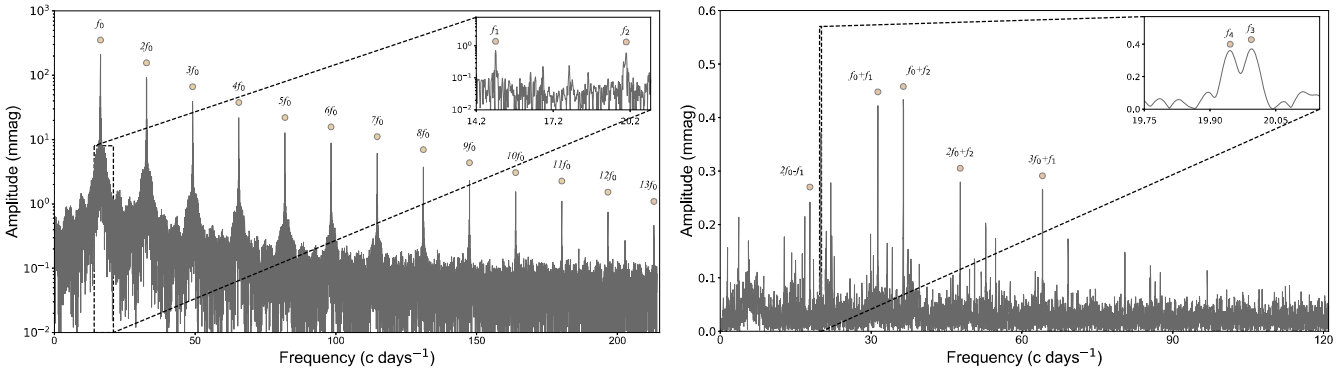

Figure 2. Frequency spectra of the light curve of CY Aqr. The left panel displays the range 0 −215 c d^{-1}, with f_0 and its harmonics, f_1 and f_2 represented. The right panel shows the range 0−120 c d^{-1}, with f_3 and f_4 represented after the removal of f_0 and its harmonics, f_1 and f_2.

Table 1
Multifrequency Solution of the Light Curves of CY Aqr from TESS (Sector 56)

No.	Marks	f (c d^{-1})	σ_f (c d^{-1})	a (mmag)	σ_a (mmag)	S/N
F1	f_0	16.383116	0.000002	212.01	0.02	18.9
F2	$2f_0$	32.766246	0.000005	92.87	0.02	19.0
F3	$3f_0$	49.14937	0.00001	39.17	0.02	18.9
F4	$4f_0$	65.53250	0.00002	22.09	0.02	18.9
F5	$5f_0$	81.91564	0.00004	12.78	0.02	18.9
F6	$6f_0$	98.29865	0.00005	8.93	0.02	18.8
F7	$7f_0$	114.68173	0.00008	6.13	0.02	18.9
F8	$8f_0$	131.0650	0.0001	3.73	0.02	18.2
F9	$9f_0$	147.4480	0.0002	2.31	0.02	17.8
F10	$10f_0$	163.8308	0.0003	1.57	0.02	17.4
F11	$11f_0$	180.2145	0.0005	1.08	0.02	16.9
F12	f_1	14.9502	0.0007	0.72	0.02	10.6
F13	$12f_0$	196.5967	0.0007	0.71	0.02	14.9
F14	f_2	20.0421	0.0007	0.71	0.02	8.7
F15	$13f_0$	212.980	0.001	0.49	0.02	13.0
F16	f_0+f_2	36.425	0.001	0.43	0.02	7.2
F17	f_0+f_1	31.334	0.001	0.42	0.02	7.5
F18	f_3	19.994	0.001	0.40	0.02	6.9
F19	f_4	19.946	0.001	0.37	0.02	8.0
F20	$2f_0+f_1$	47.717	0.002	0.28	0.02	7.4
F21	$3f_0+f_1$	64.100	0.002	0.27	0.02	6.5
F22	$2f_0-f_1$	17.816	0.002	0.24	0.02	7.2

polynomial fitting to the light curves, with uncertainties determined through Monte Carlo simulation. Furthermore, 184 new TML were derived from AAVSO data spanning 2003 to 2023, using the same methodology as for the TESS data.

For all TML data lacking inherent uncertainties, we assigned uncertainties of $20\sigma_{\rm TESS}$ for visual photometry, $5\sigma_{\rm TESS}$ for photographic observations, and $2\sigma_{\rm TESS}$ for photoelectric and CCD data (where $\sigma_{\rm TESS}=0.00005$ is the mean uncertainty of the TML from TESS), which were then incorporated into the global fitting procedure.

The $O-C$ diagram presented in W.-J. Fang et al. (2016) suggests that CY Aqr is most likely a triple system, eccentrically orbited by two low-mass companions. We fitted the TML using a quadratic function plus two sine terms, which accounts for the LTTE from two companions in independent elliptical orbits. The resulting formula for the calculated TML is

$$C = {\rm BJD}_0 + P_0\times E + \frac{1}{2}\beta E^2 + \sum_{k={\rm A,B}} A_k[\sqrt{1-e_k^2}\sin\phi_k\cos\omega_k + \cos\phi_k\sin\omega_k], \quad (6)$$

where ϕ_k ($k\equiv$ A, B) is the solution of Kepler's equation:

$$\phi_k - e_k\sin\phi_k = \frac{2\pi}{P_{\rm orb,k}}(P_0\times E - T_{0,k}). \quad (7)$$

In these equations, ${\rm BJD}_0$ denotes the initial epoch based on Barycentric Julian Day, P_0 is the pulsation period of the primary star, β represents the linear variation of the pulsation period of the primary star, $A_k = a_k\sin i_k/c$ (with c being the speed of light in vacuum) is the projected semimajor axis of the companion's orbit, e_k is the eccentricity of the companion's orbit, ϕ_k is the eccentric anomaly of the companion's orbit, ω_k (the argument of periastron) is the angle from the ascending node to periastron in the companion's orbital plane, $P_{\rm orb,k}$ is the orbital period of the companions, and $T_{0,k}$ is the time of passage through the periastron of the companions. For more details on the light-time orbit equation, refer to H.-F. Xue & J.-S. Niu (2020).

The Markov Chain Monte Carlo (MCMC) algorithm was employed to ascertain the posterior probability distribution of the parameters in Equations (6) and (7).[11] The samples of the parameters were taken from their posterior probability distribution function once the Markov Chains reached equilibrium. The mean values and standard deviations of the parameters are tabulated in Table 3, and the best-fit result (yielding χ^2/degrees of freedom = 47.05) for the $O-C$ values (excluding the linear part) along with the corresponding residuals are depicted in Figure 3.

3. Discussion and Conclusion

3.1. About the Primary Star

The asteroseismological models of the primary star of CY Aqr were constructed using the Modules for Experiments in Stellar Astrophysics (MESA; B. Paxton et al. 2011, 2013, 2015, 2018, 2019; A. S. Jermyn et al. 2023) and the stellar oscillation code GYRE (R. H. D. Townsend & S. A. Teitler 2013). Two metallicity values, [Fe/H] = −0.7 (E. Rodriguez et al. 1990) and [Fe/H] = −1.96 (Gaia Collaboration et al. 2021), corresponding to Z values of 0.003 and 0.00015 (J.-S. Niu & H.-F. Xue 2022), respectively, were incorporated into our calculation.

The luminosity and effective temperature ranges were determined following the methodology outlined in H.-F. Xue & J.-S. Niu (2020), with relevant parameters sourced from

[11] The PYTHON module `emcee` (D. Foreman-Mackey et al. 2013) is employed to perform the MCMC sampling. Some examples can be found in J.-S. Niu & T. Li (2018), J.-S. Niu et al. (2018, 2019), J.-S. Niu (2022), and references therein.

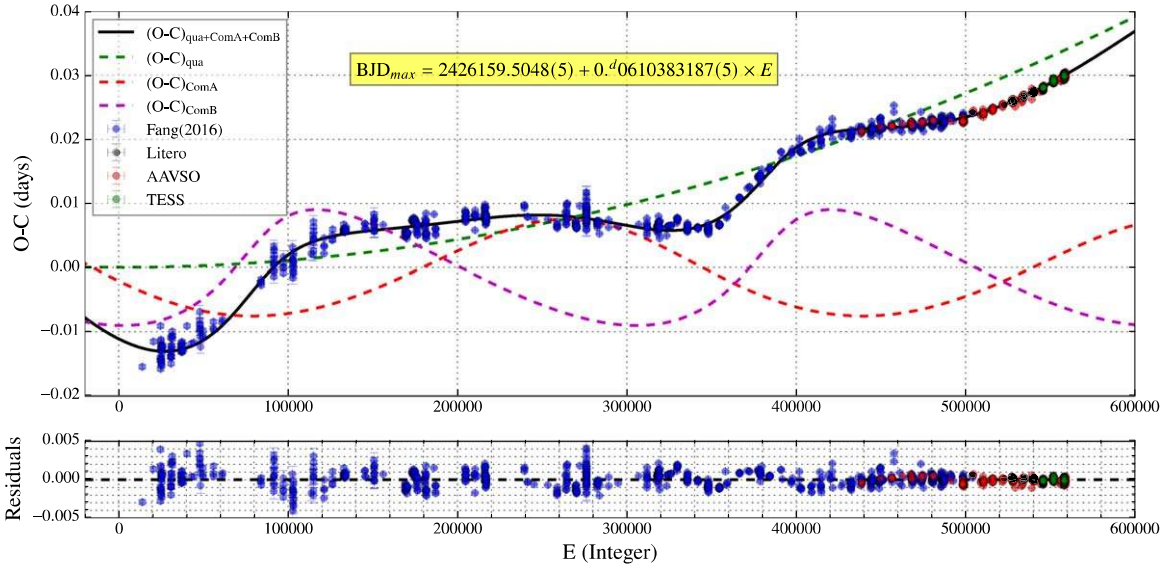

Figure 3. $O-C$ values (excluding the linear part BJD_{max}) and the corresponding residuals. In the upper panel, the black line signifies the best-fit result of a quadratic plus two light-time orbital terms, with the green dashed line indicating the quadratic component, the red dashed line indicating the light-time orbital term from Companion A, and the magenta dashed line indicating the light-time orbital term from Companion B. The lower panel displays the residuals of the best-fit result. Data from W.-J. Fang et al. (2016) are represented by blue points; historical literature data (C. Wiedemair et al. 2018, 2020) by gray points; AAVSO data by red points; and TESS data by green points.

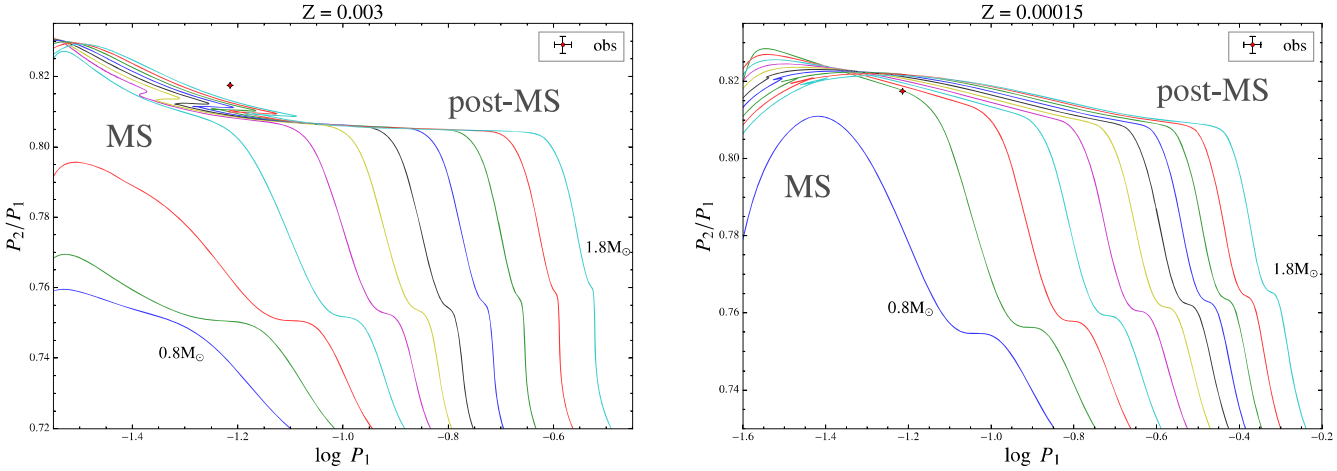

Figure 4. Petersen diagram with the observed value and all evolutionary tracks for the first and second overtone modes. The left and right panels display results for $Z = 0.003$ and $Z = 0.00015$, respectively. The observed value of the first and second overtones (F1 and F14) is indicated by a red dot with error bars. P_1 and P_2 are the periods of the first and second overtone modes (corresponding to F1 and F14), respectively.

Table 2
Pulsation Constant from Different Sources

Source	Observed Quantities				Theoretically Derived Parameters			
	$T_{\rm eff}$ (K)	log$g$ (cm s^{-2})	Distance (pc)	V (mag)	$M_{\rm bo}$ (mag)	M_V (mag)	BC	Q (days)
TESS	7351.0	4.2438	422.9060	10.99	2.4993	2.6328	−0.1334	0.0370 ± 0.0049
Gaia DR3	7153.2	3.9766	411.8049	11.04[a]	2.6071	2.7405	−0.1334	0.0271 ± 0.0011
D. H. McNamara & K. A. J. Feltz (1978)	7930	4.13	⋯	⋯	2.4	⋯	⋯	0.0330[b]
D. H. McNamara et al. (1996)	7740	4.04	⋯	⋯	2.43	2.47	⋯	0.0313[b]
J. H. Peña et al. (1999)	7500	3.91	⋯	10.7459	⋯	⋯	⋯	0.0200[b]

Notes.
[a] Here, the V-band magnitude for CY Aqr comes from the AAVSO Photometric All-Sky Survey (APASS)—Data Release, which was used to fit the Gaia model (A. A. Henden et al. 2015).
[b] All these values come from the references directly.

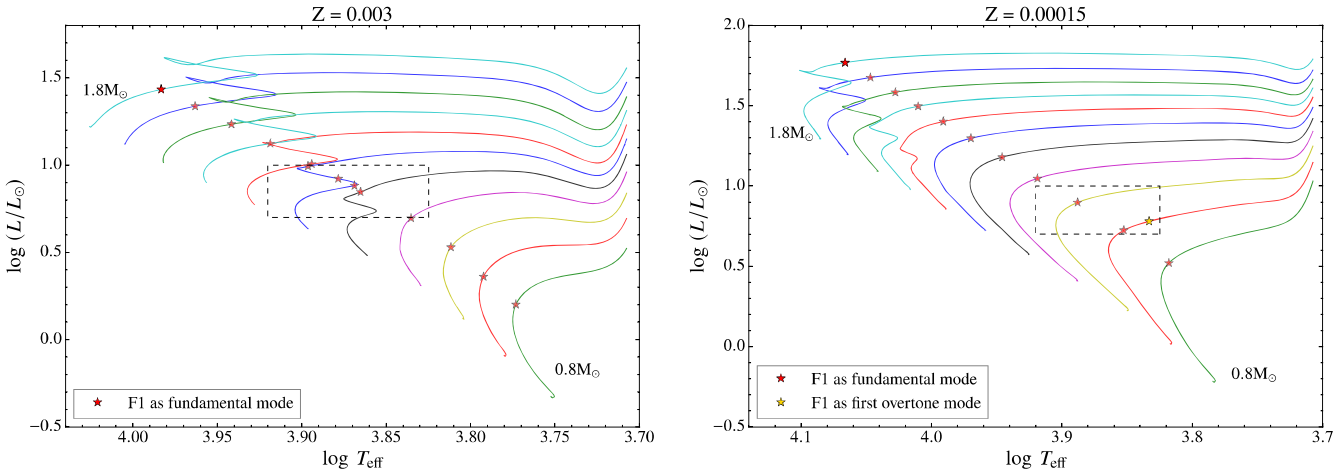

Figure 5. Best-fit seismic models superimposed on evolutionary tracks. The left and right panels display results for $Z = 0.003$ and $Z = 0.00015$, respectively. The best-fit models are indicated by pentagrams, and the dashed line boxes outline the observed luminosity and effective temperature ranges.

Table 3
Pulsating and Orbital Parameters of CY Aqr

Parameter	Value	
BJD_0	2426159.50485 ± 0.00003	
P_0 (day)	0.06103831875 ± 0.00000000006	
β (day cycle^{-1})	(2.175 ± 0.002) × 10^{-13}	
$(1/P_0)(dP_0/dt)$ (yr^{-1})	(2.132 ± 0.002) × 10^{-8}	
Parameter	Companion A	Companion B
A (day)	0.0076 ± 0.0001	0.0098 ± 0.0001
e	0.139 ± 0.002	0.431 ± 0.004
P_{orb} (days)	21990.6 ± 62.9	18547.0 ± 25.5
T_0 (BJD)	2421432.6 ± 164.8	2431156.4 ± 25.8
ω (deg)	−249.0 ± 1.6	24.5 ± 0.2
$a \sin i$ (au)	1.32 ± 0.02	1.70 ± 0.02
$f(m)$ ($M_\odot$)	0.00063 ± 0.00003	0.00190 ± 0.00006

E. F. Schlafly & D. P. Finkbeiner (2011), W.-J. Fang et al. (2016), J. H. Peña et al. (1999), and Gaia DR3. The outcomes are delineated within the dashed line box in Figure 5, with $\log L/L_\odot \in [0.70, 1.00]$ and $T_{\rm eff} \in [6680, 8320]$ K.

As that has been discussed in Section 2.2, we cannot exclude the possibility that the dominant pulsation mode could be the first overtone mode based on Q value alone. Here, we present the Petersen diagram in Figure 4 with the help of the theoretical evolutionary tracks, in which we consider F1 (f_0) and F14 (f_2) as the first and second overtone modes. In Figure 4, the theoretical evolutionary tracks pass through the observed value (the red dot) within uncertainties just when $Z = 0.00015$ and $M = 0.9\,M_\odot$, in which case F1 and F14 can be considered as the first and second overtone modes.

If we consider F1 as the fundamental mode of the primary star, we can determine the mass of it to be within the range of $0.9-1.0\,M_\odot$ and $1.2-1.3\,M_\odot$ for varying metallicities, by integrating observed constraints from the fundamental frequency, luminosity, and effective temperature. Figure 5 illustrates the best-fit seismic models alongside evolutionary tracks for different metallicities. One should note that there exist three different possible evolutionary stages when $Z = 0.003$ and $M = 1.3\,M_\odot$, which correspond to the terminal-age main sequence, the overall contraction, and the post-main-sequence evolutionary stages. All the parameters of the best-fit models (within the derived luminosity and effective temperature ranges) are listed in Table 4.

The linear period variation rates of these fitted seismic models are consistently smaller than the observed rate of $(2.132 \pm 0.002) \times 10^{-8}\,{\rm yr}^{-1}$ as presented in Table 3, suggesting that the primary star of CY Aqr may be undergoing mass loss. Employing the method proposed by H.-F. Xue & J.-S. Niu (2020), we derived the mass loss rate from the best-fit models detailed in Table 4, yielding a range from $3.36 \times 10^{-8}\,M_\odot\,{\rm yr}^{-1}$ to $6.26 \times 10^{-8}\,M_\odot\,{\rm yr}^{-1}$.

Based on the mass loss rate in main-sequence B single stars (J. Krtička 2014), we can obtain an upper limit of it in (post-) main-sequence A-F single stars as $\sim 10^{-12}-10^{-11}\,M_\odot\,{\rm yr}^{-1}$, which can be ignored comparing to the primary star of CY Aqr. Because of the lack of direct observational evidence, here we propose three possible origins of the substantial mass loss of the primary star: (i) the pulsation-induced mass loss. Although this mechanism is believed to occur in some Cepheids (L. A. Wilson & G. H. Bowen 1984), it is not yet well understood and needs more observational evidence in SX Phe stars; (ii) the mass transfer between the primary star and companions in the evolutionary history. The mass transfer will disturb the normal evolution of the primary star as a single star, which would lead to an inaccurate estimation of the evolution-induced period variation rate, and then the mass loss rate; (iii) the complexity of the three-body problem. Strictly speaking, the LTTE model we used in this work (a simple superposition of two two-body systems) is just an approximation of the real three-body system, which might be a good approximation in a short timescale, but incorrect in a long timescale. It would also lead to an inaccurate estimation of $(1/P_0)(dP_0/dt)$ and then the mass loss rate.

3.2. About the Two Companions

With the expansion of the TML and the refinement of our numerical fitting frameworks, we have, for the first time, determined the time of periastron passage T_0 and the longitude of the periastron ω for both companions. Moreover, we derived the mass functions for Companion A and B as $f(m_{\rm A}) = 0.00063 \pm 0.00003\,M_\odot$ and $f(m_{\rm B}) = 0.00190 \pm 0.00006\,M_\odot$, respectively (refer to Table 3), which are at least 1 order of magnitude larger than those obtained in W.-J. Fang et al. (2016). The differences could come from the employment of the

Table 4
Parameters of the Best-fit Models

	F1 as Fundamental Mode						F1 as First Overtone Mode
Mass ($M_\odot$)	0.9	1.0	1.2	1.3[a]	1.3[b]	1.3[c]	0.9
Z	0.00015	0.00015	0.003	0.003	0.003	0.003	0.00015
$T_{\rm eff}$ (K)	7121	7726	7331	7392	7558	7876	6810
$\log L/L_\odot$	0.72	0.90	0.85	0.88	0.92	0.99	0.78
f_0(c d^{-1})	16.3830	16.3831	16.3831	16.3832	16.3831	16.3832	16.3832[d]
$(1/P_0)(dP_0/dt)$	1.215	1.944	0.687	0.595	−2.774	10.600	2.650[e]
($\times 10^{-9}$ yr^{-1})	…	…	…	…	…	…	…

Notes.
[a] Corresponding to the terminal-age main-sequence evolutionary stage.
[b] Corresponding to the overall contraction evolutionary stage.
[c] Corresponding to the post-main-sequence evolutionary stage.
[d] Here, it is the frequency of the first overtone mode.
[e] Here, it is the period variation rate of the first overtone mode.

Table 5
Orbital Inclinations and Companion Masses of Companion A and B for Different Primary Star Masses

$M = 0.9\,M_\odot$				$M = 1.0\,M_\odot$				$M = 1.2\,M_\odot$				$M = 1.3\,M_\odot$			
$i_{\rm A}$	$m_{\rm A}$	$i_{\rm B}$	$m_{\rm B}$	$i_{\rm A}$	$m_{\rm A}$	$i_{\rm B}$	$m_{\rm B}$	$i_{\rm A}$	$m_{\rm A}$	$i_{\rm B}$	$m_{\rm B}$	$i_{\rm A}$	$m_{\rm A}$	$i_{\rm B}$	$m_{\rm B}$
6.89	1.165	10	1.158	6.89	1.224	10	1.217	6.89	1.336	10	1.329	6.89	1.389	10	1.382
13.66	0.444	20	0.442	13.66	0.472	20	0.470	13.66	0.525	20	0.522	13.66	0.550	20	0.547
20.19	0.279	30	0.277	20.19	0.297	30	0.295	20.19	0.332	30	0.330	20.19	0.348	30	0.347
26.34	0.208	40	0.207	26.34	0.222	40	0.221	26.34	0.249	40	0.247	26.34	0.261	40	0.260
31.92	0.171	50	0.170	31.92	0.182	50	0.181	31.92	0.204	50	0.203	31.92	0.215	50	0.214
36.70	0.149	60	0.148	36.70	0.159	60	0.158	36.70	0.179	60	0.178	36.70	0.188	60	0.187
40.43	0.136	70	0.135	40.43	0.145	70	0.145	40.43	0.163	70	0.163	40.43	0.172	70	0.171
42.82	0.129	80	0.129	42.82	0.138	80	0.138	42.82	0.155	80	0.155	42.82	0.163	80	0.163
43.64	0.127	90	0.126	43.64	0.136	90	0.135	43.64	0.153	90	0.152	43.64	0.161	90	0.160

Note. Unit of $i_{\rm A}$ and $i_{\rm B}$: deg (°); unit of $m_{\rm A}$ and $m_{\rm B}$: $M_\odot$.

quadratic term in Equation (6) (which is significantly nonzero), a more complete LTTE model, and the newly extended data in this work. Moreover, we suggest that a global fitting to all the free parameters simultaneously in such a problem is needed, which can help us to obtain a global optimum solution rather than local optimum solutions in most cases.

Assuming no interactions between the two companions and based on the mass function expression,

$$f(m_k) = \frac{4\pi^2 (a_k \sin i_k)^3}{G P_{{\rm orb},k}^2} = \frac{(m_k \sin i_k)^3}{(M + m_k)^2}, \tag{8}$$

we can independently determine the relationship between i_k and m_k for Companion A and B (for a given M). Setting $M = 0.9\,M_\odot, 1.0\,M_\odot, 1.2\,M_\odot, 1.3\,M_\odot$ and $i_k \in [10^\circ, 90^\circ]$, we find the mass range for the companions to be $m_{\rm A} \in [0.085, 0.818]\,M_\odot$ and $m_{\rm B} \in [0.126, 1.382]\,M_\odot$.

Considering the weak hydrogen and metallic lines near minimum light (O. Struve 1949) and the mean reddening-free color indices $(b-y)_0 \in (0.061 - 0.211)$ (corresponding to spectral types A to F) (D. H. McNamara et al. 1996), CY Aqr's companions cannot be bright red stars (which will give a obvious hydrogen or metallic lines near minimum light and significant larger value of $(b-y)_0$; J. N. Fu et al. 2008), but low-luminosity degenerate stars, such as white dwarfs, consistent with the derived mass range.

3.3. About the Triple System

However, noting that $P_{\rm orb,A} > P_{\rm orb,B}$ but $a_{\rm A} \sin i_{\rm A} < a_{\rm B} \sin i_{\rm B}$, it suggests that the orbital inclination between Companion A and B is significant and provides an additional constraint on $(i_{\rm A}, m_{\rm A})$.

Specifically, the orbital period and the semimajor axis of the orbit for Companion A and B can be expressed as

$$P_{{\rm orb},k}^2 = \frac{4\pi^2}{G(M + m_k)} a_k^3, \tag{9}$$

where G is the gravitational constant, M is the mass of the primary star, and m_k is the mass of the companions.

Based on Equation (9), we derive the orbit inclination relation between the two companions as

$$\frac{\sin i_{\rm A}}{\sin i_{\rm B}} = \frac{a_{\rm A} \sin i_{\rm A}}{a_{\rm B} \sin i_{\rm B}} \left(\frac{P_{\rm orb,B}}{P_{\rm orb,A}}\right)^{\frac{2}{3}} \cdot \left(\frac{M + m_{\rm B}}{M + m_{\rm A}}\right)^{\frac{1}{3}} \approx 0.69 \cdot \left(\frac{M + m_{\rm B}}{M + m_{\rm A}}\right)^{\frac{1}{3}}, \tag{10}$$

which establishes a relationship between $(i_{\rm A}, m_{\rm A})$ and $(i_{\rm B}, m_{\rm B})$ for a given M.

In this scenario, for a specified M, assigning a particular value to $i_{\rm B}$ yields the corresponding $m_{\rm B}$ from Equation (8) (for Companion B). By combining Equations (8) (for Companion

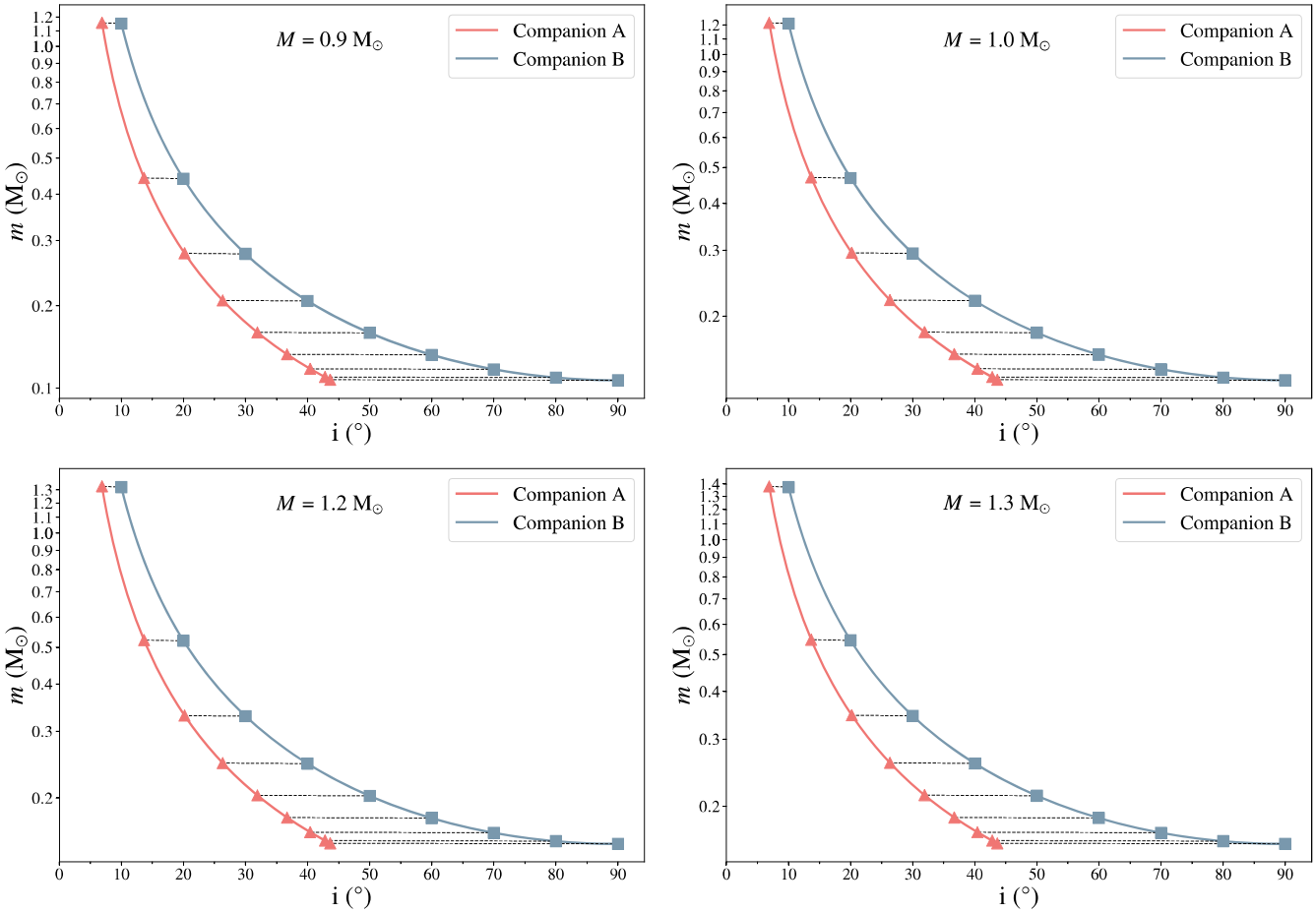

Figure 6. Relationship between the mass and the orbit inclination for Companions A and B when the mass of the primary star is $M = 0.9\,M_{\odot}$, $1.0\,M_{\odot}$, $1.2\,M_{\odot}$, $1.3\,M_{\odot}$. In each subfigure, the red line and the dark blue line represent the relationships of $(i_{\rm A}, m_{\rm A})$ and $(i_{\rm B}, m_{\rm B})$, respectively. The dark blue squares represent the anchor points when $i_{\rm B} = 10^{\circ}$, 20°, 30°, 40°, 50°, 60°, 70°, 80°, 90°, and the red triangles represent the corresponding points for Companion A, connected by dashed lines.

A) and (10), we can also determine the corresponding values of $(i_{\rm A}, m_{\rm A})$. Thus, the arrays $(i_{\rm A}, m_{\rm A})$ and $(i_{\rm B}, m_{\rm B})$ exhibit a one-to-one correspondence, significantly constraining the mass and orbital inclination of Companion A.

In Table 5, we present the one-to-one correspondence values of $(i_{\rm A}, m_{\rm A})$ and $(i_{\rm B}, m_{\rm B})$ for $i_{\rm B}$ ranging from 10° to 90° and primary star masses of $M = 0.9\,M_{\odot}$, $1.0\,M_{\odot}$, $1.2\,M_{\odot}$, $1.3\,M_{\odot}$. Based on the mass functions (Equation (8)), the relationships between $(i_{\rm A}, m_{\rm A})$ and $(i_{\rm B}, m_{\rm B})$ are depicted in Figure 6 . It is evident that the orbital inclination $i_{\rm A} \leqslant 43.^{\circ}64$, imposing a stringent constraint on the configuration of this triple system.

In a particular scenario where $i_{\rm B} = 90^{\circ}$ and BJD = 2458758.005, Figure 7 illustrates the positions of the three stars and the relationship between the orbits of Companion A and B,[12] which shows a nested structure between the orbitals.

Given that the eccentricity of Companion A (0.139 ± 0.002) is less than that of Companion B (0.431 ± 0.004) and considering the significant inclination between their orbits, we can reasonably infer that the primary star and Companion A were coevolving, while Companion B was likely captured by the primary star, subsequently intruding into the orbit of Companion A. Furthermore, considering that the eccentricity of Companion A is the smallest among similar multiple systems

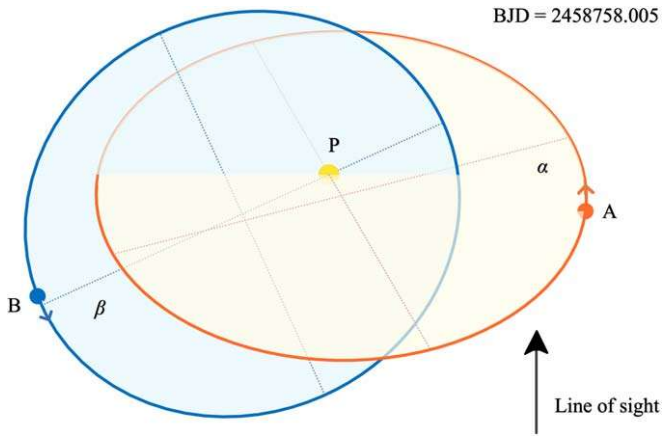

Figure 7. Positions of the three stars and the relationship between the orbits of Companion A and B when $i_{\rm B} = 90^{\circ}$ and BJD = 2458758.005. P, A, and B denote the primary star, Companion A, and Companion B, respectively. α and β denote the orbital planes of Companions A and B.

with confirmed eccentricities,[13] CY Aqr stands out as an exceedingly rare case.

However, what is even more remarkable is that the mass of Companion A is consistently slightly larger than that of

[12] Here, we also assume that the orbital planes of Companion A and B have an identical longitude of ascending node.

[13] The similar multiple systems are collected in Table A1, Appendix A; see more details therein.

Companion B, with differences of less than 1% of m_A or m_B (as seen in Table 5). When accounting for the uncertainties of the orbital parameters, Companions A and B effectively possess identical masses. Though this could be dismissed as a mere coincidence, such an explanation seems implausible.

If we believe that the system represents an inevitable and special evolutionary stage in which Companion A and B have exact masses, the evolutionary history and mass redistribution mechanism of such a system emerge as interesting enigmas. Further detailed observations of CY Aqr will be instrumental in unraveling these enigmas in the future.

Acknowledgments

H.F.X. acknowledges support from the National Natural Science Foundation of China (NSFC) (No. 12303036). All the authors acknowledge the TESS Science team and everyone who has contributed to making the TESS mission possible. We also acknowledge with thanks the variable star observations from the AAVSO International Database contributed by observers worldwide and used in this research.

All the TESS data used in this paper can be found in MAST at doi:10.17909/3GQN-PZ22.

Facility: AAVSO.

Software: `astropy` (Astropy Collaboration et al. 2013, 2018, 2022), `Lightkurve` (Lightkurve Collaboration et al. 2018), `NumPy` (C. R. Harris et al. 2020), `SciPy` (P. Virtanen et al. 2020), `matplotlib` (J. D. Hunter 2007), `emcee` (D. Foreman-Mackey et al. 2013), `Period04` (P. Lenz & M. Breger 2005), `MESA` (B. Paxton et al. 2011, 2013, 2015, 2018, 2019; A. S. Jermyn et al. 2023), `GYRE` (R. H. D. Townsend & S. A. Teitler 2013).

Appendix A
Related Works

We have collected similar systems studied by $O-C$ analysis in Table A1. More details can be referred to in the original references.

Table A1
Similar Systems Studied by $O - C$ Analysis

ID	$\frac{1}{p}\frac{dp}{dt}$ (yr^{-1})	β (day cycle^{-1})	e	$f(m)$ ($M_\odot$)	$a \sin i$ (au)	A (days)	ω (deg)	P_{orb} (days)	Type	References
BL Cam	$-2.39(8) \times 10^{-8}$	$-1.00(7) \times 10^{-13}$	0.8(7)	⋯	0.21(8)	⋯	81.29(11)	5117.0	SXP	P. Zong et al. (2019)
DY Peg	$-(5.87 \pm 0.03) \times 10^{-8}$	$(-8.55 \pm 0.04) \times 10^{-13}$	0.244 ± 0.008	$(2.47 \pm 0.12) \times 10^{-5}$	0.353 ± 0.005	0.00204 ± 0.00003	239.3 ± 5.2	$15{,}425.0 \pm 205.7$	SXP	H.-F. Xue & J.-S. Niu (2020)
KZ Hya	$(1.7 \pm 0.2) \times 10^{-7}$	$(0.17 \pm 0.02) \times 10^{-11}$	0.25 ± 0.01	0.176 ± 0.008	5.02 ± 0.010	0.029	⋯	9788.5	SXP	J. N. Fu et al. (2008)
CY Aqr[a]	$(2.132 \pm 0.002) \times 10^{-8}$	$(2.175 \pm 0.002) \times 10^{-13}$	0.139 ± 0.002 0.431 ± 0.004	0.00063 ± 0.00003 0.00190 ± 0.00006	1.32 ± 0.02 1.70 ± 0.02	0.0076 ± 0.0001 0.0098 ± 0.0001	-249.0 ± 1.6 24.5 ± 0.2	$21{,}990.6 \pm 62.9$ $18{,}547.0 \pm 25.5$	SXP	This work
DW Psc	⋯	⋯	0.40 ± 0.05	0.0405 ± 0.0073	⋯	0.0066 ± 0.0002	257.5 ± 5.1	2220.7	SXP	S. B. Qian et al. (2015)
V524 And	⋯	⋯	0.818 ± 0.002	$(3.733 \pm 0.015) \times 10^{-5}$	0.1154 ± 0.0604	0.000433 ± 0.000227	158.2 ± 44.6	2342.3	SXP	K. B. Alton & K. Stępień (2019)
BO Lyn	⋯	$(3.89 \pm 0.66) \times 10^{-13}$	0.64 ± 0.03	0.117 ± 0.013	5.19 ± 0.18	0.0300 ± 0.0011	185.5 ± 3.1	$12{,}611 \pm 36$	HADS	L.-J. Li et al. (2018)
V393 Car	5.5×10^{-6}	⋯	⋯	⋯	⋯	⋯	⋯	724.7 ± 2.0	HADS	V. Vaulato et al. (2022)
Chang 134	$(-1.8 \pm 6.6) \times 10^{-8}$	⋯	⋯	⋯	⋯	⋯	⋯	82.09 ± 0.29	HADS	V. Vaulato et al. (2022)
AN Lyn[a]	$4.5(8) \times 10^{-7}$	⋯ ⋯	⋯ ⋯	⋯ ⋯	⋯ ⋯	0.012(3) 0.025(3)	⋯ ⋯	8765.8 24,106.0	HADS	G. Li et al. (2018)
BP Peg	⋯	⋯	0 (Assumed)	$(1.9 \pm 0.5) \times 10^{-3}$	1.04 ± 0.09	0.0060 ± 0.0005	⋯	8948.4	DSCT	S. M. Wang et al. (2014)
V1162 Ori	-4.22×10^{-6}	-7.16 ± 10^{-11}	⋯	⋯	1.4	⋯	⋯	⋯	DSCT	S.-L. Kim et al. (2016)
AX UMa	⋯	$-1.135(1) \times 10^{-8}$	0.51(5)	0.459(73)	9.13(.48)	0.0527(28)	318.7(7.8)	14,877.0(119.4)	RRL	L.-J. Li et al. (2021)
V838 $\mathrm{Cyg}_{\mathrm{max}}$	⋯	⋯	0.65 ± 0.10	⋯	0.030 ± 0.004	0.000175	4.7 ± 7.7	836.3 ± 14.2	RRL	L.-J. Li et al. (2023)
TU UMa	⋯	-1.95×10^{-11}	0.663	0.046	2.91	0.0168	181.3	8510.2	RRL	J. Liška et al. (2016)
RT Aur	⋯	⋯	0 (Assumed)	0.236 ± 0.059	10.72 ± 1.56	0.0619 ± 0.0090	⋯	$26{,}429 \pm 89$	DCEP	D. G. Turner et al. (2007)

Notes. The types of primary stars are denoted as follows: SXP: SX Phoenicis variable; HADS: high amplitude δ Scuti variable; DSCT: δ Scuti variable. RRL: RR Lyrae variable. DCEP: classical Cepheids, or δ Cephei-type variables.
[a] Variable stars with two companions.

Appendix B
Long Tables

All the TML used in this work are listed in Table B1.

Table B1
Times of Maximum Light of CY Aqr

TML (BJD)	Error	Detector	Source	TML (BJD)	Error	Detector	Source	TML (BJD)	Error	Detector	Source
2427013.2934	0.0003	pg	(1)	2454749.3874	0.0001	CCD	(1)	2459833.76395	0.00003	CCD	(5)
2427413.2204	0.0003	pg	(1)	2454757.2612	0.0001	CCD	(1)	2459833.82547	0.00003	CCD	(5)
2427659.5071	0.0003	pg	(1)	2454757.3221	0.0001	CCD	(1)	2459833.88587	0.00003	CCD	(5)
2427668.9734	0.0003	pg	(1)	2454757.3832	0.0001	CCD	(1)	2459833.94711	0.00002	CCD	(5)
2427671.5303	0.0003	pg	(1)	2454761.2899	0.0001	CCD	(1)	2459834.00803	0.00004	CCD	(5)
2427671.5321	0.0003	pg	(1)	2454761.3510	0.0001	CCD	(1)	2459834.06907	0.00003	CCD	(5)
2427682.5215	0.0003	pg	(1)	2454781.2492	0.0001	CCD	(1)	2459834.13050	0.00003	CCD	(5)
2427684.9633	0.0003	pg	(1)	2454781.3098	0.0001	CCD	(1)	2459834.19107	0.00004	CCD	(5)
2427688.9910	0.0003	pg	(1)	2454796.2644	0.0001	CCD	(1)	2459834.25214	0.00003	CCD	(5)
2427690.3944	0.0003	pg	(1)	2454796.3260	0.0001	CCD	(1)	2459834.31361	0.00003	CCD	(5)

Note. The numbers in the fourth, eighth, and twelfth columns indicate the different data sources: (1) W.-J. Fang et al. (2016); (2) C. Wiedemair et al. (2018); (3) C. Wiedemair et al. (2020); (4) AAVSO; (5) TESS.

(This table is available in its entirety in machine-readable form in the online article.)

ORCID iDs

Jia-Shu Niu (牛家树) https://orcid.org/0000-0001-5232-9500
Hui-Fang Xue (薛会芳) https://orcid.org/0000-0001-6027-4562

References

Alton, K. B., & Stępień, K. 2019, AcA, 69, 283
Andreasen, G. K. 1983, A&A, 121, 250
Astropy Collaboration, Price-Whelan, A. M., Lim, P. L., et al. 2022, ApJ, 935, 167
Astropy Collaboration, Price-Whelan, A. M., Sipőcz, B. M., et al. 2018, AJ, 156, 123
Astropy Collaboration, Robitaille, T. P., Tollerud, E. J., et al. 2013, A&A, 558, A33
Bowman, D. M., Hermans, J., Daszyńska-Daszkiewicz, J., et al. 2021, MNRAS, 504, 4039
Breger, M. 1990, DSSN, 2, 13
Breger, M. 2000, in ASP Conf. Ser. 210, Delta Scuti and Related Stars, ed. M. Breger & M. Montgomery (San Francisco, CA: ASP), 3
Coates, D. W., Fernley, J. A., Sekiguchi, K., Barnes, T. G., & Frueh, M. L. 1994, MNRAS, 266, 1
Daszyńska-Daszkiewicz, J., Pamyatnykh, A. A., Walczak, P., & Szewczuk, W. 2020, MNRAS, 499, 3034
Daszyńska-Daszkiewicz, J., Szewczuk, W., & Walczak, P. 2024, MNRAS, 532, 1140
Daszyńska-Daszkiewicz, J., Walczak, P., Szewczuk, W., & Niewiadomski, W. 2023, MNRAS, 526, 1951
Derekas, A., Kiss, L. L., Bedding, T. R., et al. 2009, MNRAS, 394, 995
Eastman, J., Siverd, R., & Gaudi, B. S. 2010, PASP, 122, 935
Fang, W.-J., Luo, Z.-Q., Zhang, X.-B., et al. 2016, RAA, 16, 96
Foreman-Mackey, D., Hogg, D. W., Lang, D., & Goodman, J. 2013, PASP, 125, 306
Fu, J. N., Khokhuntod, P., Rodríguez, E., et al. 2008, AJ, 135, 1958
Fu, J. N., & Sterken, C. 2003, A&A, 405, 685
Gaia Collaboration, Brown, A. G. A., Vallenari, A., et al. 2021, A&A, 649, A1
Hardie, R. H., & Tolbert, C. R. 1961, ApJ, 134, 581
Harris, C. R., Millman, K. J., van der Walt, S. J., et al. 2020, Natur, 585, 357
Henden, A. A., Levine, S., Terrell, D., & Welch, D. L. 2015, AAS Meeting, 225, 336.16
Hunter, J. D. 2007, CSE, 9, 90
Jensch, A. 1934, AN, 253, 443
Jermyn, A. S., Bauer, E. B., Schwab, J., et al. 2023, ApJS, 265, 15
Kamper, B. C. 1985, IBVS, 2802, 1
Kim, S.-L., Cha, S.-M., Lim, B., et al. 2016, JKAS, 49, 199
Krtička, J. 2014, A&A, 564, A70
Lenz, P., & Breger, M. 2005, CoAst, 146, 53
Li, G., Fu, J., Su, J., et al. 2018, MNRAS, 473, 398
Li, L.-J., Qian, S.-B., Shi, X.-D., & Zhu, L.-Y. 2023, AJ, 166, 83
Li, L.-J., Qian, S.-B., Zhang, J., Zhu, L.-Y., & Liao, W.-P. 2018, RAA, 18, 011
Li, L.-J., Qian, S.-B., Zhu, L.-Y., He, J.-J., & Fang, X.-H. 2021, AJ, 161, 193
Lian, M. 2025, CY Aqr Data, STScI/MAST, doi:10.17909/3GQN-PZ22
Lightkurve Collaboration, Cardoso, J. V. d. M., Hedges, C., et al. 2018, Lightkurve: Kepler and TESS Time Series Analysis in Python, Astrophysics Source Code Library, ascl:1812.013
Liška, J., Skarka, M., Mikulášek, Z., Zejda, M., & Chrastina, M. 2016, A&A, 589, A94
Mahdy, H. A., & Szeidl, B. 1980, CoKon, 74, 1
McNamara, D. H. 1995, AJ, 109, 1751
McNamara, D. H., & Feltz, K. A. J. 1978, PASP, 90, 275
McNamara, D. H., Powell, J. M., & Joner, M. D. 1996, PASP, 108, 1098
Nather, R. E., & Warner, B. 1972, MNRAS, 156, 321
Nemec, J., & Mateo, M. 1990, in ASP Conf. Ser. 11, Confrontation Between Stellar Pulsation and Evolution, ed. C. Cacciari & G. Clementini (San Francisco, CA: ASP), 64
Niu, J.-S. 2022, ApJ, 932, 37
Niu, J.-S., Fu, J.-N., Li, Y., et al. 2017, MNRAS, 467, 3122
Niu, J.-S., & Li, T. 2018, PhRvD, 97, 023015
Niu, J.-S., Li, T., Ding, R., et al. 2018, PhRvD, 97, 083012
Niu, J.-S., Li, T., & Xue, H.-F. 2019, ApJ, 873, 77
Niu, J.-S., Liu, Y., & Xue, H.-F. 2023, AJ, 166, 43
Niu, J.-S., & Xue, H.-F. 2022, ApJL, 938, L20
Paxton, B., Bildsten, L., Dotter, A., et al. 2011, ApJS, 192, 3
Paxton, B., Cantiello, M., Arras, P., et al. 2013, ApJS, 208, 4
Paxton, B., Marchant, P., Schwab, J., et al. 2015, ApJS, 220, 15
Paxton, B., Schwab, J., Bauer, E. B., et al. 2018, ApJS, 234, 34
Paxton, B., Smolec, R., Schwab, J., et al. 2019, ApJS, 243, 10
Peña, J. H., González, D., & Peniche, R. 1999, A&AS, 138, 11
Percy, J. R. 1975, A&A, 43, 469
Petersen, J. O., & Christensen-Dalsgaard, J. 1999, A&A, 352, 547
Poro, A., Jafarzadeh, S. J., Harzandjadidi, R., et al. 2024, RAA, 24, 025011
Powell, J. M., Joner, M. D., & McNamara, D. H. 1995, PASP, 107, 225
Qian, S. B., Li, L. J., Wang, S. M., et al. 2015, AJ, 149, 4
Rodriguez, E., Rolland, A., & de Coca, L. 1990, Ap&SS, 169, 113
Schlafly, E. F., & Finkbeiner, D. P. 2011, ApJ, 737, 103
Smith, J. C., Stumpe, M. C., Van Cleve, J. E., et al. 2012, PASP, 124, 1000
Stassun, K. G., Oelkers, R. J., Paegert, M., et al. 2019, AJ, 158, 138
Struve, O. 1949, AJ, 54, 137
Stumpe, M. C., Smith, J. C., Catanzarite, J. H., et al. 2014, PASP, 126, 100
Stumpe, M. C., Smith, J. C., Van Cleve, J. E., et al. 2012, PASP, 124, 985
Townsend, R. H. D., & Teitler, S. A. 2013, MNRAS, 435, 3406
Turner, D. G., Bryukhanov, I. S., Balyuk, I. I., et al. 2007, PASP, 119, 1247
Vaulato, V., Nascimbeni, V., & Piotto, G. 2022, A&A, 668, A110
Virtanen, P., Gommers, R., Oliphant, T. E., et al. 2020, NatMe, 17, 261
Wang, S. M., Qian, S. B., He, J. J., Zhou, X., & Zhao, E. G. 2014, NewA, 32, 6
Wiedemair, C., Sterken, C., Eenmae, T., et al. 2018, JAD, 24, 4

Wiedemair, C., Sterken, C., Eenmae, T., et al. 2020, JAD, 26, 1
Wilson, L. A., & Bowen, G. H. 1984, Natur, 312, 429
Xue, H.-F., Fu, J.-N., Fox-Machado, L., et al. 2018, ApJ, 861, 96
Xue, H.-F., & Niu, J.-S. 2020, ApJ, 904, 5
Xue, H.-F., Niu, J.-S., & Fu, J.-N. 2022, RAA, 22, 105006
Xue, W., Niu, J.-S., Xue, H.-F., & Yin, S. 2023, RAA, 23, 075002
Yang, X. H., Fu, J. N., & Zha, Q. 2012, AJ, 144, 92
Zong, P., Esamdin, A., Fu, J. N., et al. 2019, PASP, 131, 064202